Available online at www.sciencedirect.com
SCIENCE DIRECT®
Planetary and Space Science 52 (2004) 1321–1337
Planetary and Space Science
www.elsevier.com/locate/pss

Polar observations of plasma waves in and near the dayside magnetopause/magnetosheath

J.D. Menietti*, J.S. Pickett, G.B. Hospodarsky, J.D. Scudder, D.A. Gurnett

Department of Physics and Astronomy, The University of Iowa, 210 Van Allen Hall, Iowa City, IA 52242-1479, USA

Received 26 June 2003; received in revised form 9 March 2004; accepted 30 August 2004

Abstract

The plasma wave instrument (PWI) on board the Polar spacecraft made numerous passages of the dayside magnetopause and several probable encounters with the magnetosheath during the years 1996 and 1997. During periods of relatively high density, the PWI antenna–receiver system is coupled to the plasma and oscillates. The oscillations have been shown (cf. Radio Sci. 36 (2001) 203) to be indicative of periods of higher plasma density and plasma flows, possibly associated with magnetic reconnection. We have studied the plasma waves observed on three distinct magnetopause passes distinguished by the presence of these oscillations of the PWI receivers, and we report on the data obtained near, but not during, the times of the oscillations and the possible role of these waves in magnetic reconnection. Sweep-frequency receiver and high-resolution waveform data for some of these times are presented. The plasma wave measurements on each of the passes are characterized by turbulence. The most stable waves are whistler mode emissions typically of several hundred hertz that are seen intermittently in these regions. The data indicate the presence of impulsive solitary-like wave structures with strong electric fields both parallel and perpendicular to the magnetic field near, but not always within, suspected reconnection sites. The solitary waves show the highest occurrence when observed with electrostatic electron cyclotron waves. These latter waves have been observed in the past in the cusp, polar magnetosphere, and auroral regions and therefore may represent excursions into the cusp, but also indicate the presence of low-energy electron beams. Turbulence near the lower hybrid frequency, low-frequency EM waves, and impulsive monopolar electrostatic pulses are seen throughout the magnetopause and particularly near regions of large decrease in the local magnetic field and enhanced field-aligned flows, the suspected reconnection sites. The absence of significant solitary wave signatures within suspected reconnection sites may require modifications to some reconnection models.

1. Introduction

The orbit of the Polar spacecraft was particularly well suited for long-term studies of the dayside magnetopause in 1996 and 1997. The Polar satellite was launched in late February 1996 into a polar orbit with apogee of about 9 R_E and a perigee of about 2.2 R_E, and an inclination of about 90°. During the first 2 years of operation, the orbit often allowed the satellite to travel along the magnetopause for an extended period of time. Such was the case for a well-reported event on May 29, 1996 (cf. Onsager et al., 2001; Scudder et al., 2002). The magnetopause is a region of magnetic discontinuity separating the inter-planetary magnetic field from the terrestrial magnetic field. This region has a variable thickness dependent upon the size of the currents necessary to maintain the variation or even reversal of magnetic field orientation on both sides of the magnetopause (cf. Lundin, 1988). This region is believed to play a major role in the reconnection of magnetic field lines with the subsequent injection of solar wind plasma into the magnetosphere, and is thus of particular importance.

Past studies of waves near the magnetopause and magnetosheath (cf. Anderson et al., 1982; and review by LaBelle and Treumann, 1988) have indicated intense electrostatic and electromagnetic waves. Anderson et al.

*Corresponding author. Fax: +319 335 1753.
E-mail address: jdm@space.physics.uiowa.edu (J.D. Menietti).

0032-0633/$ - see front matter © 2004 Elsevier Ltd. All rights reserved.
doi:10.1016/j.pss.2004.08.003

reported a very low-frequency continuum, short wavelength "spikes", and whistler mode emissions. During a flux transfer event that these authors reported, additionally, quasi-periodic electron cyclotron harmonics correlated with ~1 Hz magnetic fluctuations. Most recently, Pickett et al. (2001) have presented observations of plasma waves observed by Polar in the cusp turbulent boundary layer. These authors confirmed the observations of Anderson et al. (1982) and showed high-resolution waveforms indicative of non-linear processes near reconnection sites. We will report further on all of these emissions using recent high-resolution Polar plasma wave observations.

The plasma wave instrument (PWI) on board the Polar spacecraft made numerous passages of the dayside magnetopause and likely encounters with the magnetosheath during the years 1996 and 1997. Swept-frequency receiver and high-resolution waveform data for some of these times are presented. The data indicate the presence of impulsive solitary-like wave structures with strong electric fields both parallel and perpendicular to the magnetic field, regions of significant local decreases in the ambient magnetic field associated with turbulent lower-hybrid-like waves.

LaBelle and Treumann (1988) have summarized the role of wave turbulence in providing sufficient diffusion to support reconnection or boundary layer formation. Based on magnetopause wave observations and amplitudes at the time, these authors found diffusion coefficients were generally too small for the ion acoustic mode, the modified two-stream instability, the lower hybrid drift instability, and the electron cyclotron drift instability.

The question of the source of the dissipation necessary to decouple the motion of ions and electrons and allow magnetic reconnection has had recent progress. Treumann et al. (1995) have argued that lower hybrid waves were always able to provide sufficient resistivity. Cattell et al. (1995) provided observational evidence of examples of these waves with sufficient amplitude to support this theory. These waves are damped at high values of β (ratio of plasma particle to magnetic field pressure), i.e., near the x-line, but it has been suggested they occur near enough to the diffusion region to supply the necessary resistivity.

Lower hybrid waves have also been the subject of studies of Bale et al. (2002), who sought to determine the importance of anomalous resistivity of lower hybrid waves in the generalized Ohm's law. These authors found the contribution of lower hybrid drift instability anomalous resistivity to the parallel electric field to be essentially insignificant. Thus the pressure and inertial terms of the generalized Ohm's law appear to be of dominant importance in magnetic reconnection at the Earth's magnetopause, unless higher-frequency waves come into play.

Drake et al. (2003) have recently shown via 3-D Vlasov simulations of current-driven instabilities that electron holes and particle energization result from magnetic reconnection. This association was suggested earlier by Pottelette and Treumann (1998). The simulations demonstrate the growth of the Buneman instability, which leads directly to the development of electron holes. These electron holes result in electron scattering, but this scattering is not consistent with what has traditionally been referred to as anomalous resistivity. The saturation of the electron hole generation is linked to the development of lower hybrid waves whose field-aligned phase speed matches that of the electron hole. Drake et al. (2003) and Cattell et al. (2002) have reported the Polar observations of electron holes and lower hybrid waves from the electrostatic field instrument (EFI), but the observations are quite localized, resulting from the so-called "burst-mode" of the EFI instrument (cf. Harvey et al., 1995). This mode operates to store the largest event electric field data to accumulate the "best" events, but consequently does not record continuous data. It is of importance to observe the wave environment for an extended region along the magnetopause, which PWI can do in a limited way as will be described.

When an interplanetary magnetic cloud impinges upon the terrestrial magnetosphere, it produces local high densities, bulk flows, and may initiate magnetic reconnection. During such periods, the PWI preamplifiers frequently experience oscillations due to coupling between the plasma and the antenna. Recently, Kolesnikova and Béghin (2001) have shown that these periods of feedback oscillations observed sometimes in the Polar Plasma Wave Investigation antenna–receiver–plasma system during magnetopause encounters are indicators of high density and bulk flows, and may be indicative of magnetic reconnection. Kolesnikova and Béghin (2001) have shown by analytic modeling that the instability conditions can be satisfied for ~10 eV electron flow with a density of ~100/cm^3 and a bulk flow velocity of ~200 km/s. In this paper, we report on a study of three passes which were encounters with the magnetopause/magnetosheath (MP/MS) near regions when the PWI experienced oscillations, thus indicating the presence of high-density flows, probably associated with magnetic reconnection. We have concentrated on data near, but not within, regions of such oscillations. We will discuss the wave observations and their possible role in the reconnection processes.

2. Instrumentation

Polar is the first satellite to have three orthogonal electric antennas (E_u, E_v, and E_z), three triaxial magnetic search coils, and a magnetic loop antenna, as well as an

advanced Plasma Wave Instrument (PWI) (Gurnett et al., 1995). This combination can potentially provide the polarization and direction of arrival of a signal without any prior assumptions.

The PWI on the POLAR spacecraft is designed to provide measurements of plasma waves in the Earth's polar regions over the frequency range from 0.1 Hz to 800 kHz. Five receiver systems are used to process the data: a wideband receiver, a high-frequency waveform receiver (HFWR), a low-frequency waveform receiver (LFWR), two multichannel analyzers, and a pair of sweep-frequency receivers (SFRs). The SFR has a frequency range from 26 Hz to 808 kHz in five frequency bands. The frequency resolution is about 3% at the higher frequencies. In the log mode, a full frequency spectrum can be obtained every 33 s. From 12.5 to 808 kHz, a full frequency spectrum can be obtained every 2.4 s. The wideband receiver (WBR) provides high-resolution waveform data, and is programmable allowing the selection of 11, 22, or 90 kHz bandwidths with a lower band edge (base frequency) at 0, 125, 250, and 500 kHz. In the 90 kHz bandwidth mode the sampling rate is 249 kHz. The LFWR measures electric and magnetic field waveforms in the frequency range of 0.1–25 Hz at a 100 Hz sampling rate. The duty cycle of this receiver is typically to take a 2.5 s snapshot of data every 25 s. The HFWR measures waveform data over the frequency range of 20 Hz to 25 kHz, but also operates with a 2 or 16 kHz filter. The sampling rate is 71.43 kHz in the 25 kHz mode. Typically, the receiver obtains a 0.5 s snapshot of data every 128 s, but often every 9 s.

The electron and ion hot plasma instrument (HYDRA) (Scudder et al., 1995) is a three-dimensional hot plasma instrument for the POLAR spacecraft. It consists of a suite of particle analyzers that sample the velocity space of electron and ions between ~2 and 35 keV/q in three dimensions, with a routine time resolution of 0.5 s. The instrument has been designed specifically to study accelerated plasmas such as in the cusp and auroral regions.

3. Observations

3.1. May 29, 1996

We will examine in some detail plasma wave data for three MP/MS passes. Each pass is characterized by greater than usual plasma density near the magnetopause, which is indicated by the presence of oscillations of the SFR plasma wave receiver. The first pass we will discuss is that of May 29, 1996, when Polar was traveling northward on the dayside almost parallel to the MP (cf. Plate 1 of Onsager et al., 2002). In Fig. 1, we display the electric (top) and magnetic (bottom) field data for the SFR for a 5 h period of the MP/MS pass of May 29, 1996. The white line depicts the local electron cyclotron frequency (f_{ce}). The frequency range of both panels is 27 Hz–200 kHz. Oscillations of the SFR are characterized by broadbanded emissions (particularly noticeable in the electric field data) with intense emission close to the local plasma frequency. Note the narrowbanded emission near 90 kHz in the electric field data. These oscillations have been shown to be due to enhanced plasma density and bulk flows (cf. Kolesnikova and Béghin, 2001). Also significant in this plot are the frequent, impulsive decreases in f_{ce}, indicating local drops in the magnetic field intensity. Overall, the entire time interval is characterized by turbulent and intense emission at $f<f_{ce}$ that is both electrostatic and sometimes electromagnetic. In the lower panel of Fig. 1, we see the increase in bandwidth of EM emission for $f<100$ Hz that is associated with decreases in f_{ce} (or magnetic field). These emissions include both whistler mode and Alfvenic emissions.

In Fig. 2, we show a higher-resolution plot of the electric field data for this pass for the time interval from 03:30 to 07:30. The periods of oscillation of the preamplifiers are seen along with the turbulent nature of f_{ce}. We will discuss in more detail some of the high-resolution data obtained during time periods other than those for which oscillations of the SFR occur: near 05:12 where electrostatic electron cyclotron (EEC) emission occurs; near 05:05:30 where some well-defined whistler mode emission exists; and also in the interval 06:44–07:10 where a large decrease of f_{ce} exists.

Due to the enormous amount of data that exists, we are forced to display only a few plots of characteristic waveforms present at various times within the pass. In Fig. 3a, we show waveform data obtained from the HFWR for a 57 ms period starting at 05:11:58.793 UT. We note that this time interval is not characterized by the most significant decreases in ambient magnetic field, nor is it near what is believed to be a magnetic reconnection diffusion region, near 07:03 (cf. Scudder et al., 2002). The top three panels are the tri-axial electric field data while the bottom three panels are the corresponding magnetic field data. Significant in this figure are the solitary wave structures seen in the third panel ($E_{\parallel}$) with magnitudes of about 0.6 mV/m. These impulsive waves are said to be due to a bi-stream instability (Goldman et al., 1998, 1999), but Drake et al. (2003) also suggest that they may result directly from the development of the Buneman instability and strong parallel electric fields associated with reconnection. The solitary wave signatures are not universally present throughout this pass, but are seen most predominately associated with EEC waves. The lower three panels of Fig. 3a show turbulent, low-frequency electromagnetic (EM) waves with a frequency of roughly 60 Hz, which are probably in the whistler mode. The EEC waves and

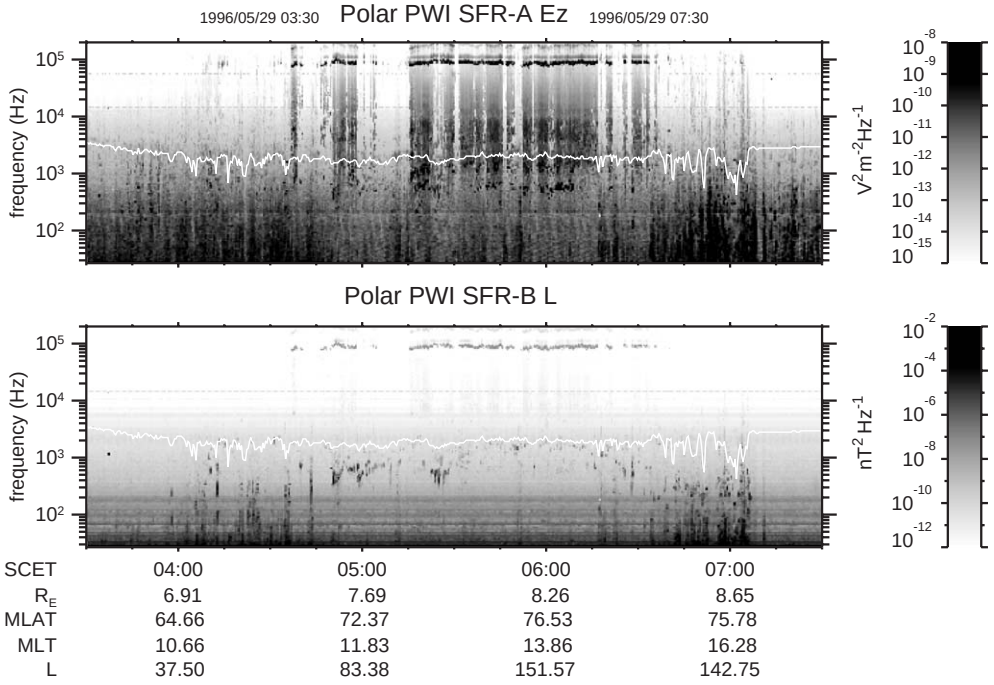

Fig. 1. Electric (top) and magnetic (bottom) field data for the SFR for a 5 h period of the MP/MS pass of May 29, 1996. The white line depicts the local electron cyclotron frequency (f_{ce}). The frequency range of both panels is 27 eV–200 kHz. Note the intense emissions near 80 kHz and above, which are due to oscillations of the PWI pre-amplifier, which occur during high density conditions, possibly indicative of nearby magnetic reconnection.

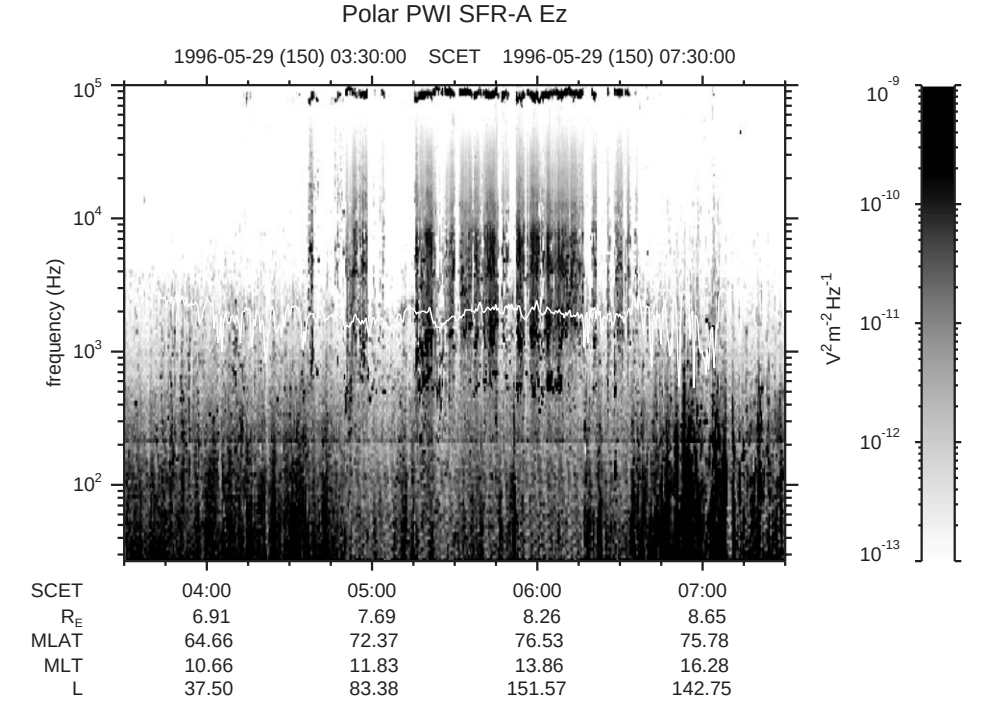

Fig. 2. A higher-resolution plot of the electric field data for the pass of Fig. 1, for the time interval from 03:30 to 07:30. The periods of oscillation of the pre-amplifiers are seen (near 80–90 kHz) along with the turbulent nature of f_{ce}.

harmonics are not discernable in Fig. 3a, because the HFWR was operating in a mode with an upper frequency limit of less than 2 kHz. However, we have wideband data just prior to this time period shown in Fig. 3b. This is a frequency-vs.-time spectrogram for a 48 s time interval starting at 05:10:24.870. The frequency

scale is linear from 0 to about 11 kHz (with a roll-off filter at higher frequencies). Note the presence of the EEC waves near 2 kHz and at harmonic (ECH). The broadbanded bursts are due to the presence of solitary wave structures as seen in Fig. 3a.

Anderson et al. (1982) reported ECH oscillations at the magnetopause. Farrell et al. (1990) and Menietti et al. (2001, 2002) more recently have shown that EEC waves and harmonics are observed in the cusp, polar magnetosphere, and auroral regions and are believed to be generated by low-energy electron beams. Hence their presence in this pass suggests the presence of electron beams and/or brief excursions of the satellite out of the MP/MS and into the cusp/magnetosphere. The presence of low-energy electron beams is indicated in Fig. 4, which is a plot of the electron energy density for pitch angles in the range $0^\circ < a < 30^\circ$ (bottom panel) and the electron anisotropy (top) for the time interval 05:00–05:15. These data are obtained from the particle instrument, HYDRA, on board Polar (cf. Scudder et al., 1995). The anisotropy indicates the difference between field-aligned and perpendicular spectra. Field-aligned and field-opposed spectra are averaged (with equal weights) and compared to the perpendicular spectrum in units of expected error. In the interval from about 05:09:45 to about 05:12:30, there is a clear increase in the parallel electron flux and anisotropy for $E < 200$ eV.

In Fig. 5, we show another 57 ms snapshot of waveform data starting at 05:05:32.048. Here is a rare instance of well-organized waves in what is otherwise

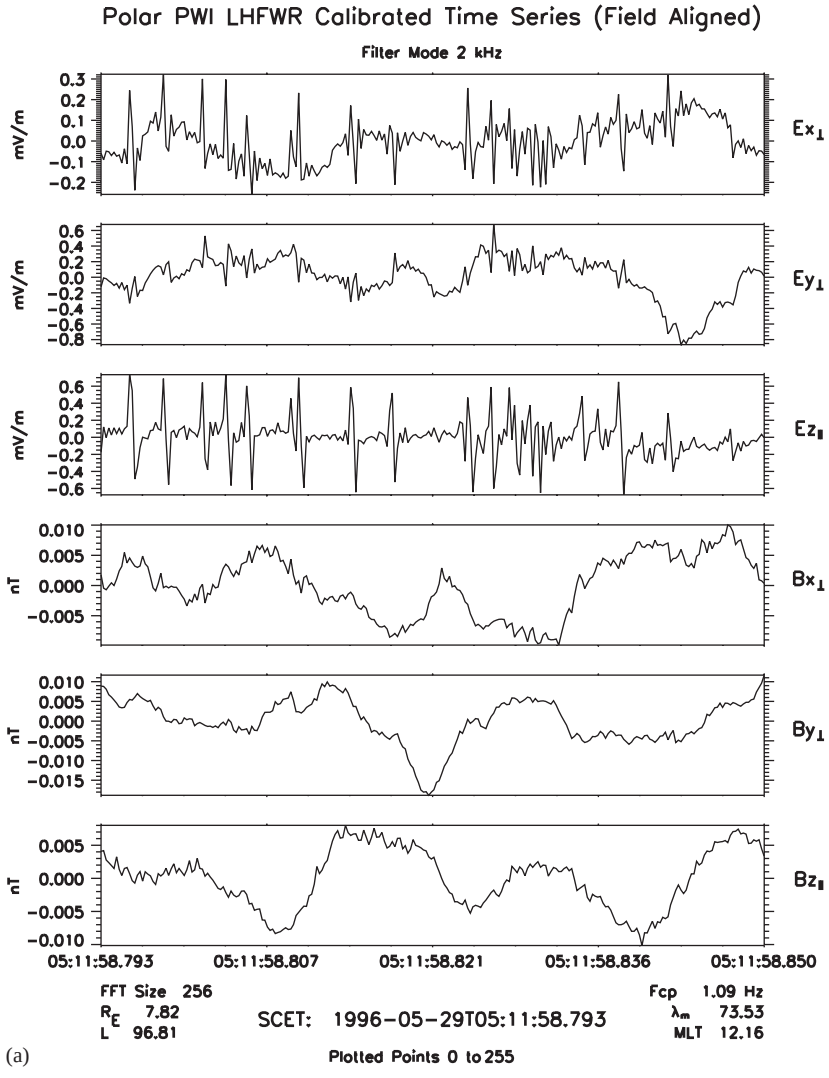

Fig. 3. (a) Waveform data obtained from the HFWR for a 57 ms period starting at 05:11:58.793 UT. The top three panels are the tri-axial electric field data while the bottom three panels are the corresponding magnetic field data. Significant in this figure are the solitary wave structures seen in the third panel ($E_\parallel$) with magnitudes of about 0.6 mV/m. (b) A 48 s, high-resolution f-vs.-time spectrogram of the wideband electric field data. The start time for the plot is specified next to the gray scale. The times are given relative to the start time. The frequency range is from 0 to about 11 Hz with a roll-off filter at higher frequencies. Note the harmonics of the EEC emissions. The superposed, spiky wideband bursts are primarily due to solitary wave structures.

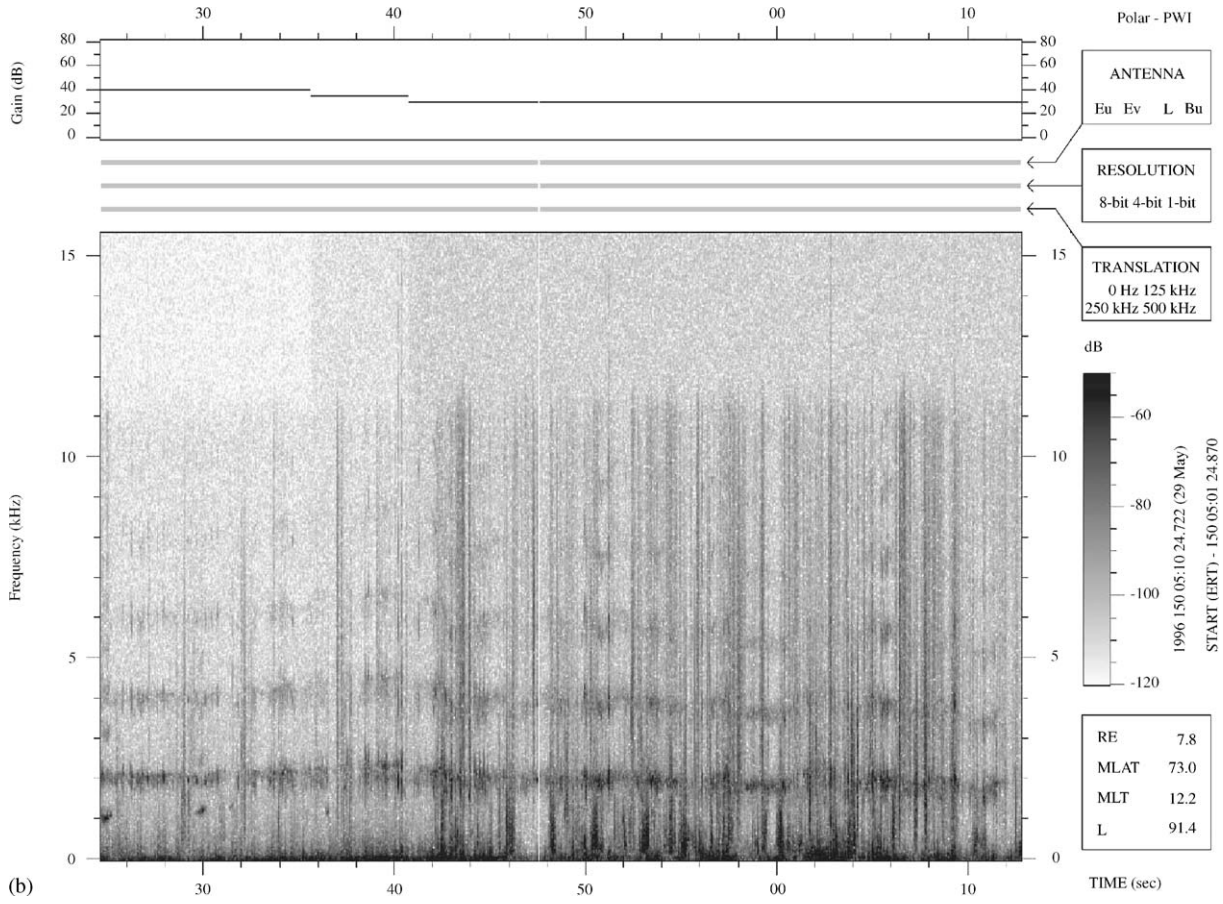

Fig. 3. (*Continued*)

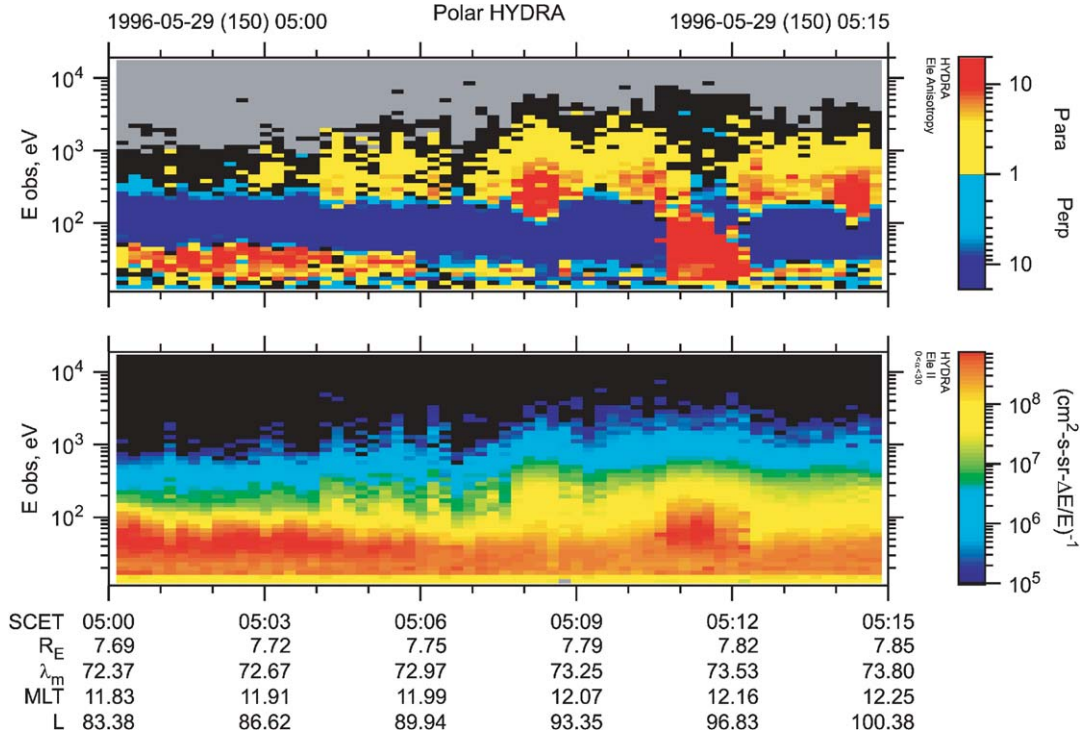

Fig. 4. The electron energy flux from HYDRA is shown in the lower panel for the time period shown. The data have been sorted for pitch angles in the range $0^\circ < a < 30^\circ$. There is a significant increase in the energy of the most intense electron flux for the period from about 05:09:45 to 05:12:15, during which EEC waves are observed (Fig. 3). The top panel displays the electron anisotropy (defined in the text), and clearly shows the presence of field-aligned electrons during the same interval (05:09:45–05:12:15).

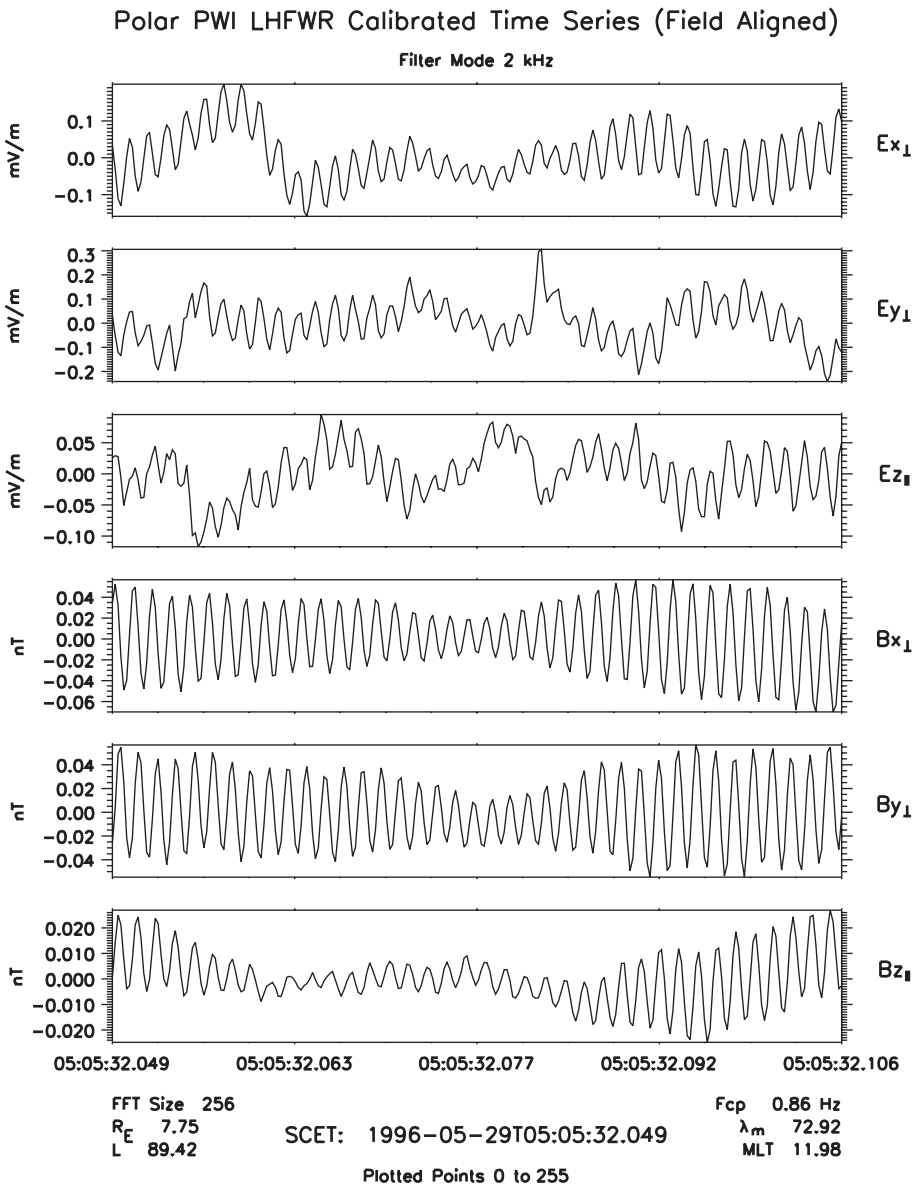

Fig. 5. A 57 ms snapshot of waveform data starting at 05:05:32.048. Here is a rare instance of well-organized waves in what is otherwise dominantly turbulent emission. These sinusoidal waves have a dominant frequency of about 690 Hz (whistler mode) and a much lower modulating frequency (seen best in panels 1 and 6) with a frequency of roughly 50 Hz.

dominantly turbulent emission. These sinusoidal waves have a frequency of about 690 Hz (whistler mode) and a much lower modulating frequency (seen best in panels 1 and 6) with a frequency of roughly 50 Hz, although it is not clear if the lower frequency is truly electromagnetic.

We have performed an analysis of the Poynting vector for the waves seen in Fig. 5. At this time the Poynting flux is directed in the generally field-opposed direction at an angle of approximately 140° with respect to the magnetic field. Since the magnetic field at this time is directed northward, this means the whistlers are likely directed toward the Earth.

In the time interval 06:40–07:15 UT, there are significant periods of impulsive decreases in f_{ce}. The local DC magnetic field data (not shown) indicate impulsive changes of direction of B_z and/or B_y (GSM) during this period. At 06:45, $B_z \sim +42$ nT, but drops rapidly to ~ -75 nT near 06:46 and rises rapidly again to $\sim +50$ nT near 06:47:30. In Fig. 6, we display a multipanel plot of HYDRA data for a 15-min time interval centered near 06:47. The panels are (top to bottom) ion skew, electron skew, downward ions, upward ions, downward electrons, and upward electrons. Here, downward is toward Earth (for $-B_z$). Skew is defined as the difference between magnetic field-aligned and field-opposed fluxes at fixed energy. Skew is made dimensionless by dividing by the expected errors in the fluxes compared. Seen in the data centered near

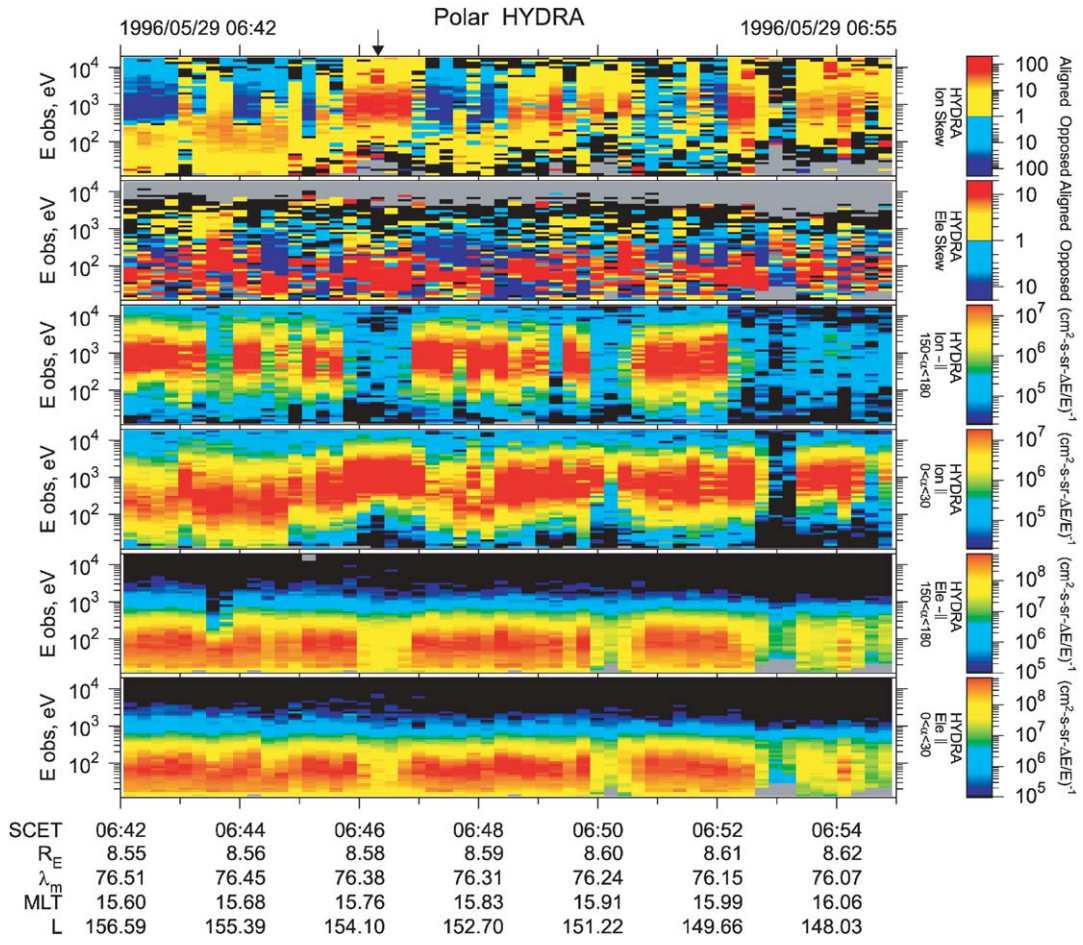

Fig. 6. Multipanel plot of HYDRA data for a 15 min time interval centered near 06:47. The panels are (top to bottom) ion skew, electron skew, downward ions, upward ions, downward electron, and upward electrons. Here downward is toward Earth (for $-B_z$). Skew is defined in the text. The region of enhanced field-aligned flow is indicated with an arrow at the top of the plot.

06:46:20 (and indicated with an arrow) is a burst of intense field-aligned ions (toward Earth) followed immediately by a burst of field-opposed ions. These strong flows are no doubt observed at lower altitudes. The plasma waves near this time period include an increase in the bandwidth of low-frequency waves for $f<100$ Hz, consistent with whistler mode, magnetosonic, and Alfven wave emission.

We now investigate some of the lower-frequency waves observed by the PWI LFWR, which measures waves in the frequency range from 0.1 Hz to about 25 Hz. The most significant difference between these waves and those measured by HFWR at higher frequencies are the wave amplitudes. This receiver was operating in a mode that took 2.5 s snapshots every 25 s. In Fig. 7 we show a snapshot of waves which demonstrate turbulence levels at typically an order of magnitude higher in intensity. For a 2.5 s time period starting at 06:46:38.6, in the center of the ion field-aligned burst region indicated in Fig. 6, we note a turbulent structure with a significant impulse observed in the electric field $E_\perp$ direction (panel 1), which has a perpendicular component with an amplitude of approximately 20 mV/m. We point out that it was more common to find these impulsive wave structures with $E_\perp > E_\parallel$. The turbulent electric field has a quasi-frequency of about 16 Hz and also with $E_\perp > E_\parallel$. At this time the local lower hybrid frequency for an O^+ plasma is about 14.6 Hz and for an He^+ plasma is ~29 Hz. For a plasma of H^+ the lower hybrid frequency is about 58 Hz, which is higher than the upper cutoff frequency of the LFWR. The HFWR data at this same time period (not shown) indicate a turbulent plasma with an irregular frequency of ~50 Hz. The last three panels depict the turbulent magnetic field waveforms, with an amplitude of ~2 nT in each of the field-aligned components. The irregular waves have frequencies ~1 Hz, which suggests the waves are magnetosonic or ion cyclotron waves (f_{cH}~1.4 Hz).

3.2. Pass of April 1, 1997

The next MP/MS pass we consider is that of April 1, 1997. In Fig. 8 we present, in the same format as Fig. 1,

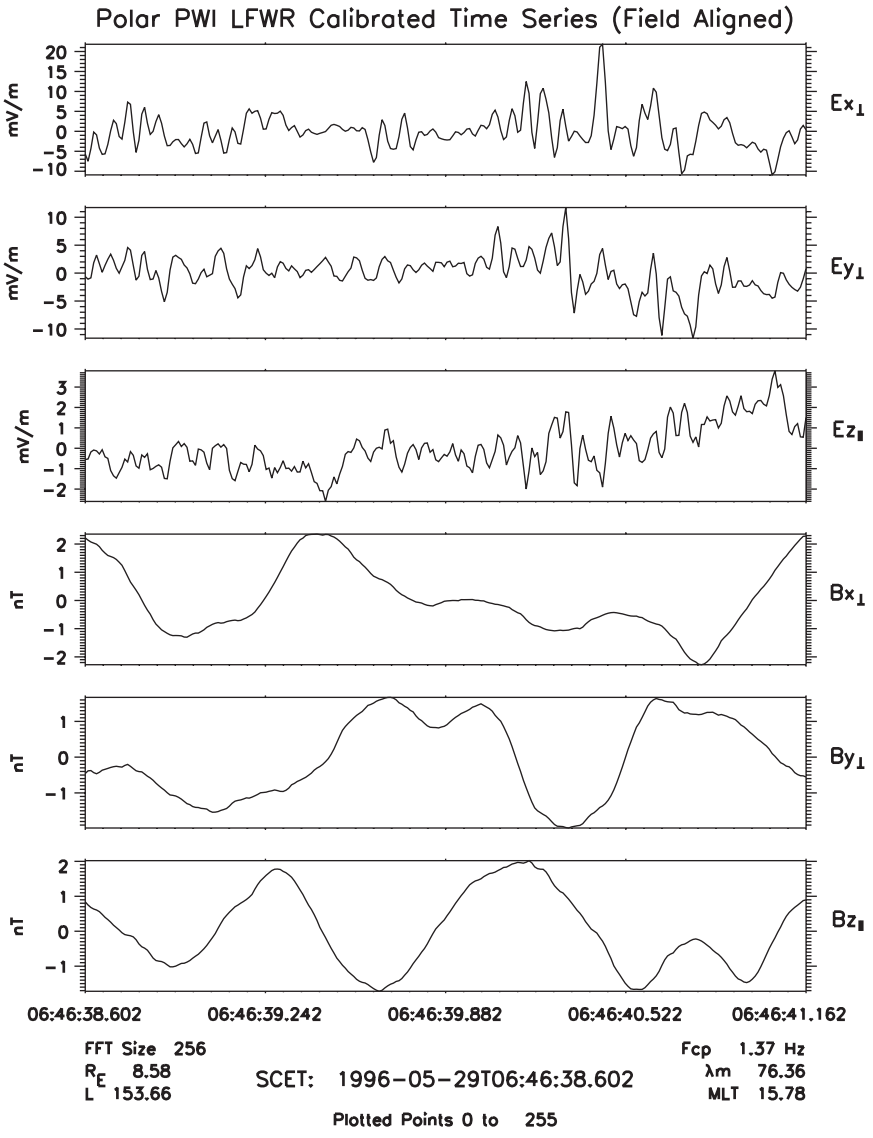

Fig. 7. Waveform electric and magnetic field data for a 2.5 s time period starting at 06:46:38.6, in the center of the ion field-aligned burst region indicated in Fig. 6. Note a turbulent structure with a significant impulse observed in the electric field $E_{\|}$ direction (panel 1) which has a perpendicular component with an amplitude of approximately 20 mV/m.

the electric and magnetic field data of the SFR. The oscillation of the receiver, an indication of high local density and enhanced bulk flows, is seen in the intervals from about 06:46 to 06:48 and 06:50:30 to 06:54:30. The local magnetic field is seen to be very turbulent (note the value of f_{ce}), with many impulsive decreases. Overall, the waves look similar to those of Fig. 1 for May 29, 1996. The magnetic field oscillations (Fig. 8, lower panel) show intermittent enhancements of EM waves at frequencies less than ~200 Hz and amplitudes of several nT as we also saw in Fig. 1.

In Fig. 9, we depict the HFWR data (with an upper cutoff frequency of 2 kHz at this time) for a 57 ms snapshot starting at 06:14:26.177. The data are in the same format as Fig. 3a. We have chosen this time period within the region of turbulent magnetic field because it shows three types of significant waveforms commonly seen in these regions. Higher-frequency EEC waves just above the cyclotron frequency are seen in the first half of the top three panels of electric field data. The oscillations are at a frequency of ~1430 Hz while f_{ce}~1400 Hz. In panel 3 ($E_{\|}$), a few solitary wave structures are indicated. These are commonly seen associated with the EEC waves. In all six panels, one observes the lower-frequency electromagnetic whistler mode at f ~215 Hz. The wideband electric field data for this time period (not shown, but similar to Fig. 3b), clearly show the EEC waves and harmonics superposed with many broad-banded spiky emissions that are largely due to solitary wave bursts.

Data from the LFWR for frequencies less than 25 Hz in many ways look similar to Fig. 7. There are turbulent

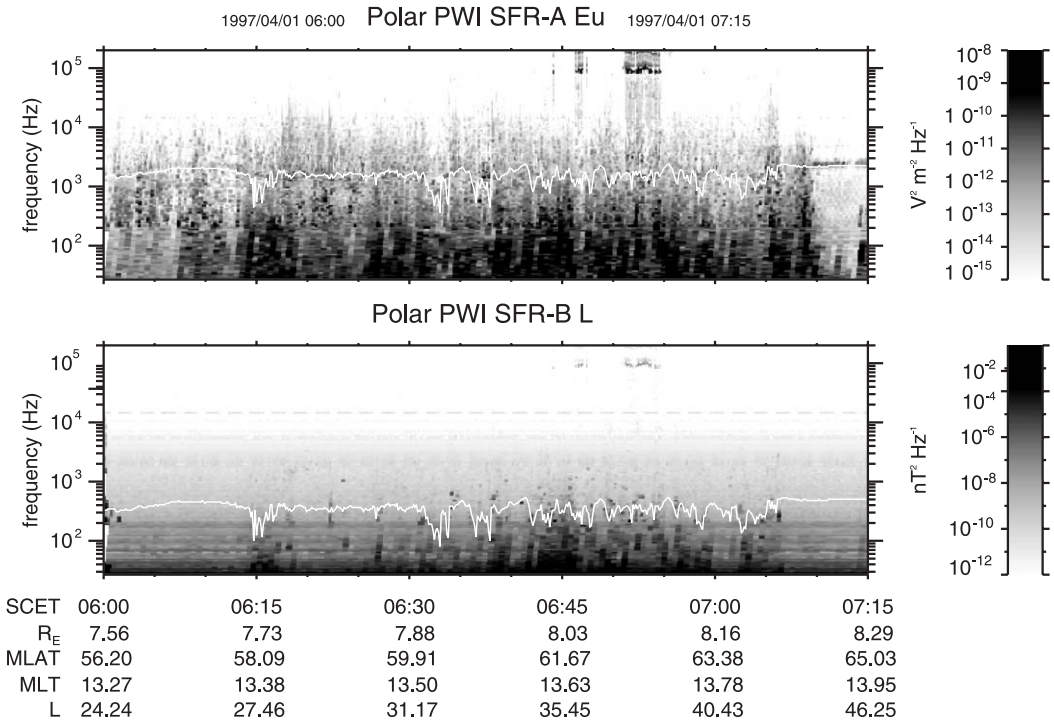

Fig. 8. We present, in the same format as Fig. 1, the electric and magnetic field data of the SFR for April 1, 1997. The turbulence of the period is seen in the erratic depressions of the local electron cyclotron frequency (white line). There is much similarity between this figure and Fig. 1.

electric field emissions with a characteristic frequency near 15 Hz (the local lower hybrid frequency is ~16.5 Hz for an He^+ plasma and ~8.3 Hz for an O^+ plasma), and there are also turbulent EM emissions with f~1 Hz, which are ion cyclotron or magnetosonic waves (locally, f_{cH} ~0.8 Hz).

In Fig. 10, we display the energy flux for field-aligned electrons (bottom panel), field-opposed electrons (panel 2) and similarly for the ions (panels 3 and 4), centered on the time near 06:15. This is the time where there are large fluctuations in ambient magnetic field (cf. Fig. 8). Clearly there is a substantial increase in ion energy up to 10 keV near this time, while the electrons show a similar inverted-V structure but with energies up to about 1 keV. In the top two panels of Fig. 10, we display the ion and electron skew for the same time period. Significant in this plot is the indication of large low-energy field-opposed fluxes of both ions and electrons just prior to about 06:14 followed by large higher-energy field-aligned ions and electrons centered near 06:15.

3.3. Pass of June 22, 1997

Fig. 11 presents the electric and magnetic field data for the MP/MS pass of June 22, 1997. As can be seen, the oscillations of the SFR occur at many places during this pass, indicating areas of relatively high density and bulk flows. There is a region of particularly large local decreases in the magnetic field centered near 03:00. EEC waves are observed just prior to the region of turbulent magnetic field at ~02:21 UT. The EEC waves were also pointed out in the other two passes and we believe they are indicative of low-energy electron beams and/or excursions into the cusp/magnetosphere.

In Fig. 12, we show waveforms from the HFWR in the same format as before (i.e., Fig. 3a), but at this time the high-frequency cutoff is 25 kHz. The EEC waves are indicated in the second panel with a maximum magnitude of about 0.05 mV/m. Also present associated with the EEC waves are solitary wave structures with amplitudes of perhaps 0.4 mV/m. These observations are similar to those observed for other MP/MS passes, and show the direct correspondence of the EEC waves and the solitary wave structures.

Each of the passes examined exhibits periods of impulsive magnetic field reversals in B_z or B_y. These reversals are significant because they are sometimes associated with particle flow reversals. Another example occurs near 02:50 where the ambient DC magnetic field rapidly changes from approximately −40 nT to ~0 and then peaks at about +25 nT near 02:51. Then the B-field rapidly decreases to about −30 nT near 02:52. We examine the electron and ion energy flux and skew for a period centered near 02:51 in Fig. 13 (same format as before). We see a narrow region of enhanced field-aligned flow amidst a region of field-opposed flow corresponding to these

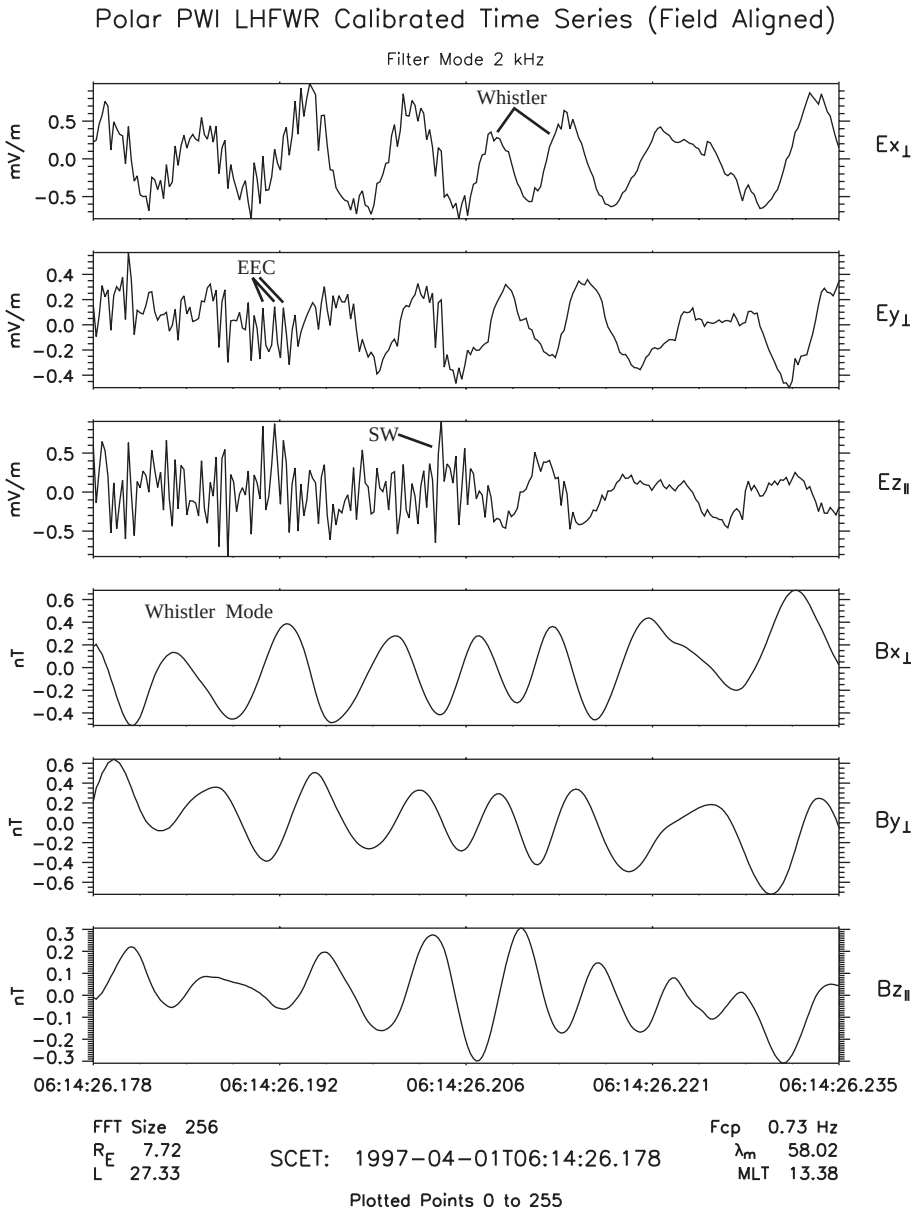

Fig. 9. HFWR data (with an upper cutoff frequency of 2 kHz at this time) for a 57 ms snapshot starting at 06:14:26.177. During this time period, note the high-frequency EEC waves in the first three panels ($t<$06:14:26:.21), several examples of solitary wave bursts in panel 3, and electromagnetic whistler mode seen in all panels, particularly in the magnetic field data.

magnetic field direction reversals. In Fig. 14, we present the electric and magnetic field data at this time from the HFWR for 29 ms snapshot starting at 02:51:07.244. The electric field data show unusual impulsive signals in both $E_{\parallel}$ and $E_{\perp}$ that have a magnitude of >0.1 mV/m. There also appears to be a weak whistler mode wave with a frequency of about 70 Hz.

4. Summary and discussion

We have presented plasma wave data from the PWI on the Polar satellite for three MP/MS passes. For each of these passes, there is evidence of intense wave turbulence in the form of impulsive electric fields. Characteristic of MP/MS passes are relatively high densities. During such periods, the PWI pre-amplifiers frequently experience oscillations due to coupling between the plasma and the antenna. We have identified regions of magnetic field impulsive decreases to relative low values and regions of relatively strong field-aligned plasma flows as regions that are near reconnection sites.

The data show generally turbulent emissions throughout the magnetopause region. Seen intermittently are large-amplitude Alfven and magnetosonic waves at $f<1$ Hz and amplitudes frequently exceeding several

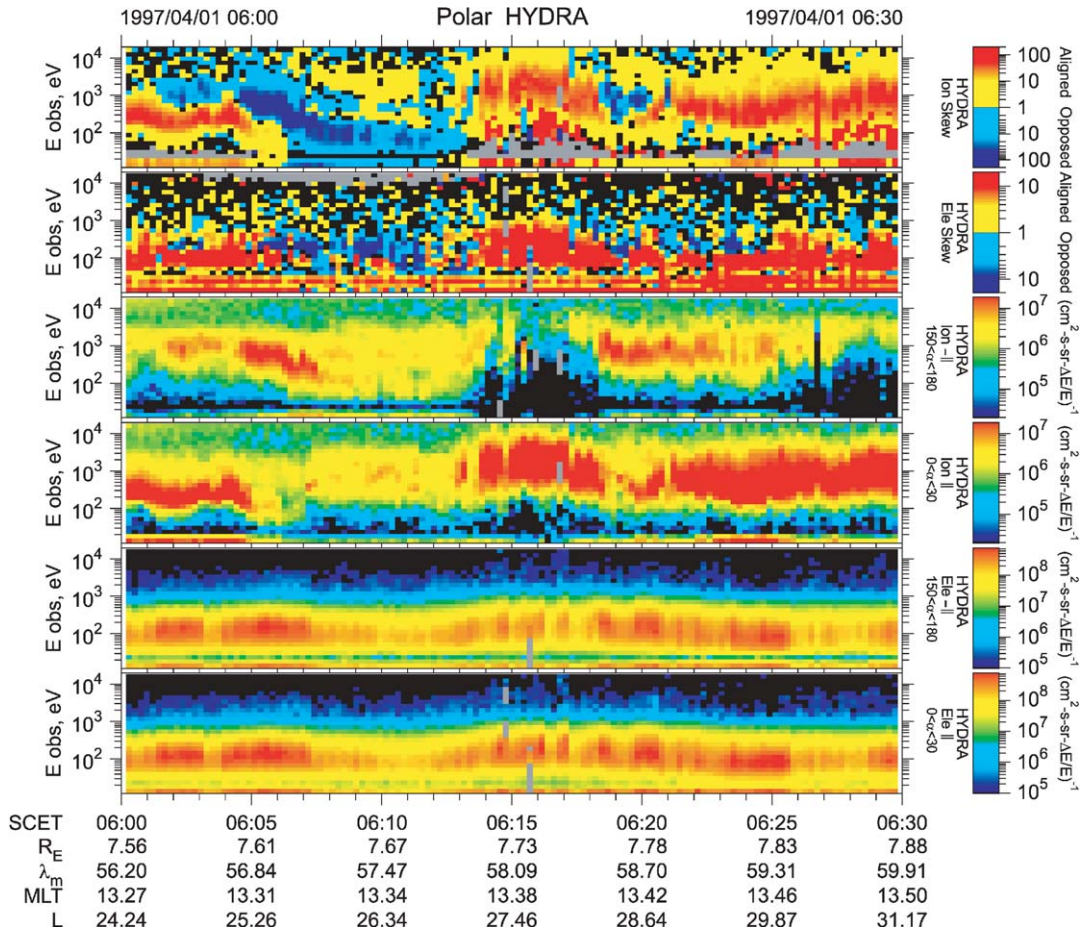

Fig. 10. Energy flux for field-aligned electrons (bottom panel), field-opposed electrons (panel 2) and similarly for the ions (panels 3 and 4), centered on the time near 06:15, where there are large fluctuations in ambient magnetic field. In the top two panels of Fig. 10, we display the ion and electron skew for the same. Note the large low-energy field-opposed fluxes of both ions and electrons just prior to about 06:14 followed by large higher-energy field-aligned ions and electrons centered near 06:15.

nT, ion cyclotron waves of similar amplitudes; turbulent lower hybrid-like waves at $f<30$ Hz (generally) and amplitudes of typically several mV/m; strong whistler mode waves at frequencies of a few hundred Hz to 1 kHz with electric field amplitudes that can be a few tenths of mV/m; and strong EEC waves at $f\sim2$ kHz. Solitary wave structures are seen intermittently, but especially near regions of EEC waves. Solitary waves have amplitudes of typically 0.5 to several mV/m when observed at $f>25$ Hz by the HFWR, but significantly higher amplitudes (tens of mV/m) when observed at $f<25$ Hz by the LFWR. Near the more turbulent regions (large ambient magnetic field decreases), we sometimes observe significant electric field "pulses" of magnitude tens of mV/m and time a duration of 0.1–0.2 s. The presence of the EEC waves may be important in future theoretical studies. These waves have been observed by Polar in the cusp and polar magnetosphere, and are believed to grow due to the presence of low-energy electron beams in those regions. When these waves are observed in the present study, they appear to be within regions of open magnetic field, cusp-like plasmas. As pointed out by Winske et al. (1995), the electron cyclotron drift instability saturates at low levels due to magnetic field gradients. This could explain why ECH oscillations are not easily observed near regions where f_{ce} displays rapid decreases, and may preclude any observations of these waves near a magnetic x-line.

Drake et al. (2003) have reported the presence of solitary waves that develop from the Buneman instability, resulting from the relative drift of electrons and ions. The waves in Drake et al. (2003) are near $f\sim f_{pe}$ in a plasma with $f_{pe}<f_{ce}$. However, as PWI observes and as Drake et al. concede, f_{pe} is greater than f_{ce} near the magnetopause. It will be interesting to determine the impact of future simulations using more realistic plasma parameters. The spacing of the electron holes in the simulations of Drake et al. is controlled by the parallel structure of the lower hybrid waves. PWI observes

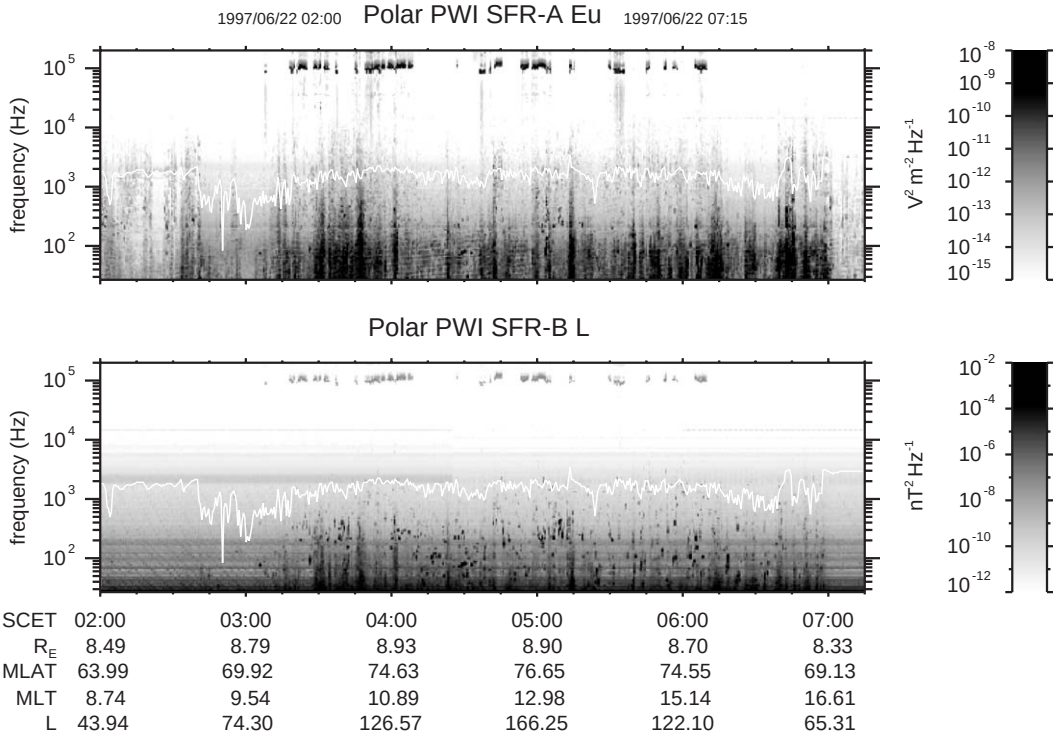

Fig. 11. Electric and magnetic field data for the MP/MS pass of June 22, 1997. As can be seen, the oscillations of the pre-amplifiers occur at many places during this pass, indicating places of relatively high density and bulk flows.

emissions with frequencies close to f_{LH} for large periods of time near the magnetopause. Umeda et al. (2002) have also shown that electrostatic simulations of solitary waves that lower hybrid mode waves are generated near the source of electron beams and that these waves couple with the electron holes to modulate their propagation.

We estimate that the plasma wave power levels (watts) are typically about 1% of the total particle power. However, the isolated and impulsive electric fields (~20 mV/m) can locally have much higher energy density than the particles. An important question has been the role of waves to provide the necessary diffusion to sustain the lower latitude boundary layer in the absence of reconnection or to provide anomalous resistivity in the diffusion region required to break the magnetic field frozen-in condition, decoupling the motion of ions and electrons allowing reconnection. We can estimate this role for the Polar observations. Coroniti (1985), LaBelle and Treumann (1988), Treumann et al. (1995), and Winske et al. (1995) have all reported the diffusion coefficients for a number of wave modes including the lower hybrid drift instability (LHDI) and the electron cyclotron drift mode instability (ECDI). LaBelle and Treumann (1988) state that

$$D_\perp = \left(\frac{\pi}{8}\right)^{1/2}\left(\frac{m_i}{m_e}\right)\left(\frac{T_i}{T_e}\right)\rho_e^2\omega_{LH}\frac{\varepsilon_0\delta E^2}{2nT_i} \quad \text{LHDI}, \tag{1}$$

$$D_\perp = \frac{3}{7}\rho_e^2\omega_e\frac{\varepsilon_0\delta E^2}{4nT_i} \quad \text{ECDI}, \tag{2}$$

where subscripts i and e refer to ions and electrons, respectively, ρ_e is the electron gyroradius, ω_{LH} is the lower hybrid frequency, δE is the electric field amplitude, ω_e is the electron plasma frequency, and n is the plasma density.

Likewise, Tsurutani and Thorne (1982) have calculated the diffusion coefficient necessary for low-frequency electromagnetic emission ($f \sim$ ion cyclotron frequency, f_{cH}):

$$D_\perp \sim 2\left(\frac{\delta B}{B}\right)^2 D_{max} \quad \text{EM}, \tag{3}$$

where

$$D_{max} = \frac{\xi_\perp c}{2eB} \tag{4}$$

and $\xi_\perp$ is the ion resonant energy, and δB is the oscillating magnetic field amplitude.

To estimate these values based on the Polar observations, we have concentrated on wave observations in the interval 07:02 to 07:06, near the probable diffusion region for the pass of May 29, 1996, (cf. Scudder et al., 2002). Near 07:02:18 on this pass, we observe lower hybrid emission with typical oscillating electric field magnitudes of up to 10 or 15 mV/m, along with

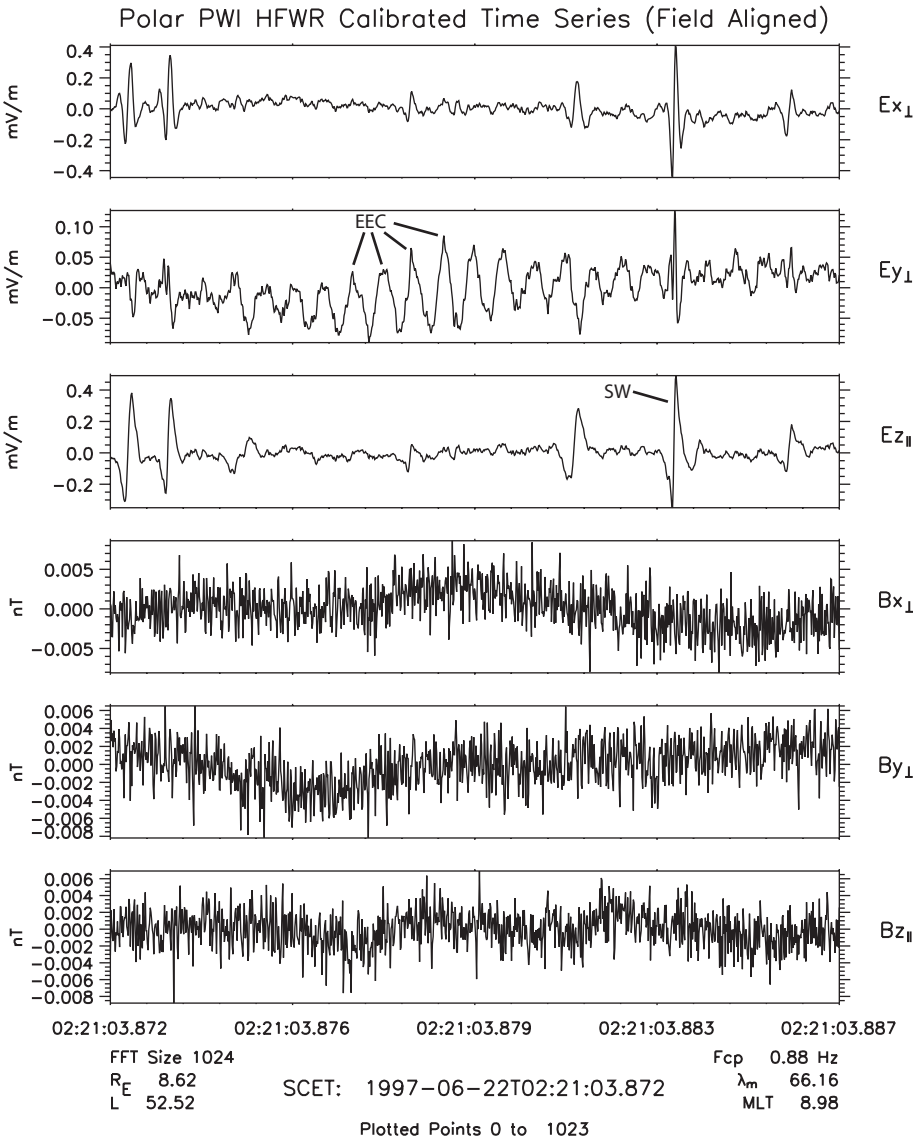

Fig. 12. A higher-resolution plot of the electric field data of this region. EEC waves are indicated just prior to the region of turbulent magnetic field.

low-frequency magnetic oscillations ($f \sim 2\, f_{cH}$) of magnitude ~4 nT. Near this region at about 07:05:45, we observe EEC waves with magnitudes of about 1 mV/m.

We believe that we are near the reconnection sites at times on each of the passes discussed in this paper. We can make an estimate of the diffusion time across the diffusion region, where reconnection should take place, as $\tau = L^2/D_\perp$ where L is the width of the diffusion region. Traditionally, this value is chosen to be on the order of the ion inertial length or ion gyroradius. LaBelle and Treumann (1988) have acknowledged that L could be of the order of the electron gyroradius, and more recently Scudder et al. (2002) have argued this to be the case from Polar observations. We have calculated τ assuming L is the ion inertial length ($L = 50$ km), and the results are summarized in Table 1.

The LHDI and EM emission are within an order of magnitude of the value required to sustain the lower latitude boundary layer in the absence of reconnection, $10^9\ m^2\ s^{-1}$ (Sonnerup, 1980). The EEC waves are much too low in amplitude to be effective. We do observe solitary wave structures imbedded within the EEC waves, but not frequently within the suspected reconnection site. We may crudely estimate $D_\perp$ for solitary waves (SW) using the expression for electrostatic waves given by Tsurutani and Thorne (1982),

$$D_\perp = 2(\Delta E/B)^2 (c/v_{th})^2 D_{max},$$

where v_{th} is the particle thermal velocity. For 500 eV particles, and assuming $\Delta E \sim 1$ mV/m, we obtain $D_\perp \sim 1.9 \times 10^8\ m^2/s$ (ions) and $10^5\ m^2/s$ (electrons). The ion diffusion is comparable to the values above for

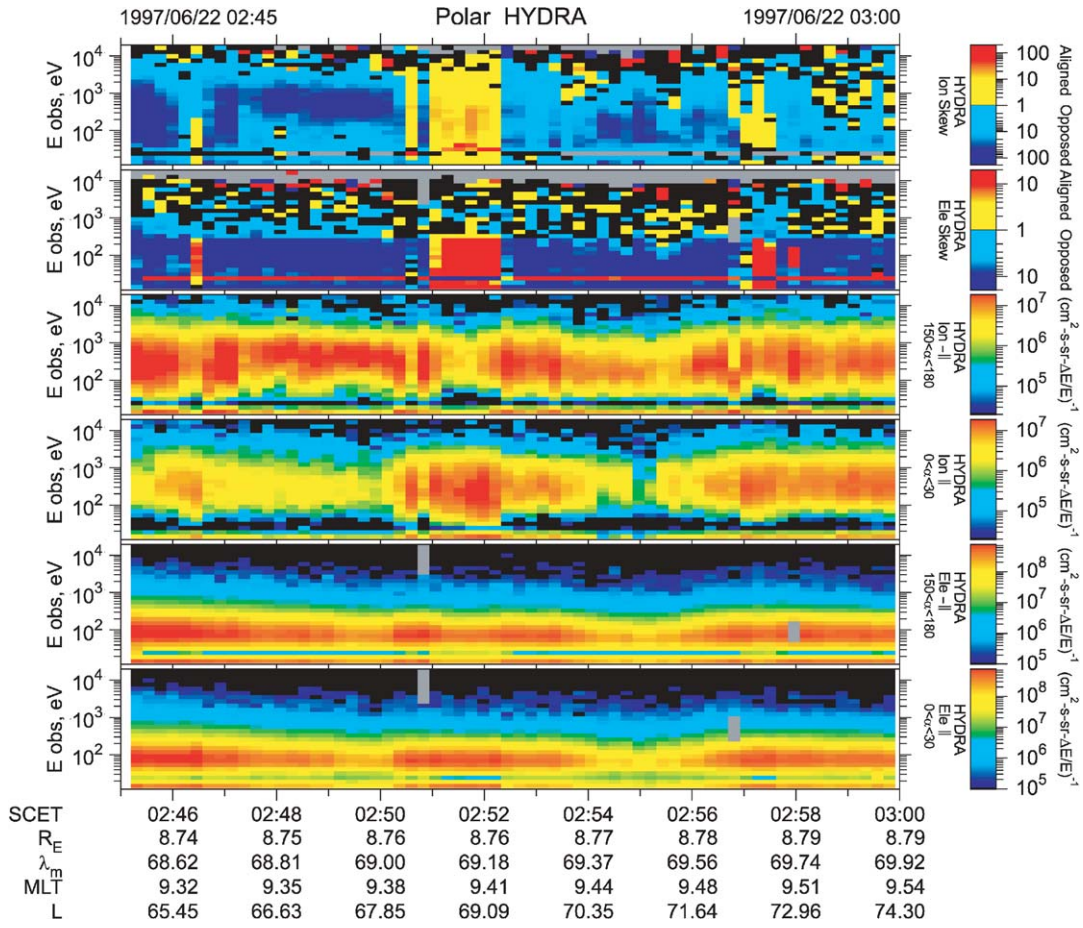

Fig. 13. Electron and ion energy flux and skew for a period centered near 02:51. Note the narrow region of enhanced field-aligned flow amidst a region of field-opposed flow corresponding to magnetic field direction reversals.

lower hybrid and low-frequency EM waves. The diffusion times shown in Table 1 for LHDI and EM waves are short enough to explain observed reconnection rates (on the order of minutes), based on polar orbiting low-altitude satellite observations of cusp ion injections. The possibility remains that the contribution of the waves to the diffusive resistivity is due to the combined effects of different wave modes.

5. Conclusions

The purpose of this paper was to perform a comparative analysis of the plasma wave data from a series of MP/MS passes which show a likelihood of near encounters with the magnetic reconnection site. In doing so we have been able to confirm the observations of a number of past studies, but also we have been able to pose some new questions. The plasma wave receiver on board Polar is unique in its ability to obtain extremely high-resolution waveform data from three electric and three magnetic antennas. The sheer volume of this data has provided a problem of data assimilation and display. The approach taken in this paper was to take snippets of exemplary datasets for display and comment.

In each dataset from the three passes, Polar PWI observed regions of complex low-frequency turbulence that increased in bandwidth and intensity near regions of impulsive ambient magnetic field that decreased to low values locally (possible reconnection sites). Within these regions, the HYDRA particle data indicate regions of strong field-aligned flows. Within these flow regions, the PWI observes a number of different wave topologies, intermittently, including whistler mode and low-frequency Alfvenic modes, but on every example PWI observed lower hybrid turbulence. Solitary waves were observed occasionally within the regions of strong flow, but not consistently. Rather, large monopolar impulsive waves are typically seen in these regions. Solitary waves with the highest occurrence frequency and the largest amplitude occurred near, but not within, the flow regions of dynamic magnetic field oscillations and associated strongly with EEC waves. The lack of solitary wave structures within the reconnection site is an important observation because the studies of Drake et al. (2003), for instance, suggest they should play a vital role in particle dynamics. It will be important

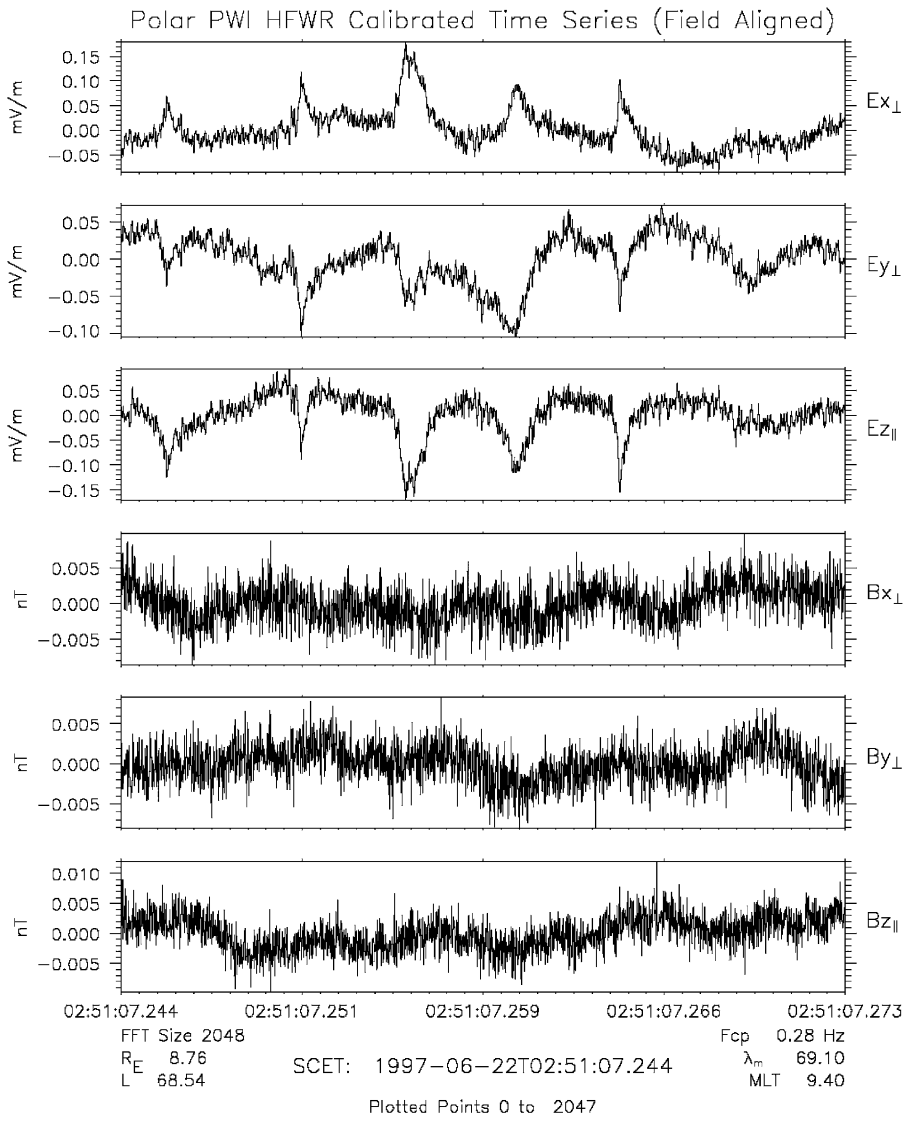

Fig. 14. Electric and magnetic field data from the HFWR for a 29 ms snapshot starting at 02:51:07.244. The electric field data show unusual impulsive signals in both $E_{\parallel}$ and $E_{\perp}$ that have a magnitude of >0.1 mV/m.

Table 1
Diffusion times

Wave mode	$D_{\perp}$ (m^2/s)	τ_i (s)
LHDI	2×10^{8}	12.5
ECDI	2×10^{1}	1.25×10^{8}
EM	1.5×10^{8}	16.7

to use appropriate ion to electron mass ratios as well as the ratio of f_p/f_{ce} in future theoretical studies of reconnection.

The calculated values of diffusion times must be taken with caution. The diffusion coefficients are based on linear theory and wave growth rates, but the physics of the diffusion region and reconnection is very non-linear. Some diffusion times in Table 1 are reasonable to explain known reconnection rates, but it is not certain that the wave observations were taken precisely within the diffusion region. It will also be important to separate temporal from spatial fluctuations in the wave data. Scudder et al. (private communication, 2004) are developing new analysis techniques for single spacecraft which will be able to distinguish compressible slow or fast magnetosonic waves in the magnetic field data. We also look forward to future results from multi-satellite missions such as Cluster, which are now beginning to resolve these issues.

Acknowledgments

This work was supported by NASA Grants NAG5-9561 and NAG5-11942. We wish to thank

J. Hospodarsky for assistance in typesetting, and A. Persoon for assistance with some of the figures.

References

Anderson, R.R., Harvey, C.C., Hoppe, M.M., Tsurutani, B.T., Eastman, T.E., Etcheto, J., 1982. Plasma waves near the magnetopause. J. Geophys. Res. 87, 2087–2107.

Bale, S.D., Mozer, F.S., Phan, T., 2002. Observation of lower hybrid drift instability in the diffusion region at a reconnecting magnetopause. Geophys. Res. Lett. 29, 33–36.

Cattell, C., Wygant, J., Mozer, F.S., Okada, T., Tsuruda, K., Kokubun, S., Yamamoto, T., 1995. ISEE-1 and Geotail observations of low frequency waves at the magnetopause. J. Geophys. Res. 100, 11823–11830.

Cattell, C.A., Crumley, J., Dombeck, J., Wygant, J.R., Mozer, F.S., 2002. Polar observation of solitary waves at the Earth's magnetopause. Geophys. Res. Lett. 29 (5), 1065.

Coroniti, F., 1985. Space plasma turbulent dissipation: reality or myth? Space Sci. Rev. 42, 399–410.

Drake, J.F., Swisdak, M., Cattell, C., Shay, M.A., Rogers, B.N., Zeiler, A., 2003. Formation of electron holes and particle energization during magnetic reconnection. Science 299, 873–877.

Farrell, W.M., Gurnett, D.A., Menietti, J.D., Wong, H.K., Lin, C.S., Burch, J.L., 1990. Wave intensifications near the electron cyclotron frequency within the polar cusp. J. Geophys. Res. 95, 6493–6504.

Goldman, M.V., Oppenheim, M.M., Newman, D.L., 1998. PIC simulations of bipolar wave structures driven by dense beams in the auroral ionosphere. In: Chang, T., Jasperse, J.R. (Eds.), Physics of Space Plasmas 15. MIT Center for Theoretical Geo/Cosmo Plasma Physics, Cambridge, MA, pp. 115–120.

Goldman, M.V., Oppenheim, M.M., Newman, D.L., 1999. Nonlinear two-stream instabilities as an explanation for auroral bipolar wave structures. Geophys. Res. Lett. 26, 1821–1824.

Gurnett, D.A., Persoon, A.M., Randall, R.F., Odem, D.L., Remington, S.L., Averkamp, T.F., DeBower, M.M., Hospodarsky, G.B., Huff, R.L., Kirchner, D.L., Mitchell, M.A., Pham, B.T., Phillips, J.R., Schintler, W.J., Sheyko, P., Tomash, D.R., 1995. The Polar plasma wave instrument. Space Sci. Rev. 71, 597–622.

Harvey, P., Mozer, F.S., Pankow, D., Wygant, J., Maynard, N.C., Singer, H., Sullivan, W., Anderson, P.B., Pfaff, R., Aggson, T., Pedersen, A., Falthammar, C.-G., Tanskannen, P., 1995. The electric field instrument on the Polar satellite. Space Sci. Rev. 71, 583–596.

Kolesnikova, E., Béghin, C., 2001. Instability problem of the electric field antennas on the Polar spacecraft. Radio Sci. 36, 203–221.

LaBelle, J., Treumann, R.A., 1988. Plasma waves at the dayside magnetopause. Space Sci. Rev. 47, 175–202.

Lundin, R., 1988. On the magnetospheric boundary layer and solar wind energy transfer into the magnetosphere. Space Sci. Rev. 48, 263–320.

Menietti, J.D., Pickett, J.S., Gurnett, D.A., Scudder, J.D., 2001. Electrostatic electron cyclotron waves observed by the plasma wave instrument on board Polar. J. Geophys. Res. 106, 6043–6057.

Menietti, J.D., Santolik, O., Scudder, J.D., Pickett, J.S., Gurnett, D.A., 2002. Electrostatic electron cyclotron waves generated by low-energy electron beams. J. Geophys. Res. 107 (A10), 1285.

Onsager, T., Scudder, J.D., Lockwood, M., Russell, C., 2001. Reconnection at the high-latitude magnetopause during the northward interplanetary magnetic field conditions. J. Geophys. Res. 106, 25467–25488.

Pickett, J.L., Franz, J.R., Scudder, J.D., Menietti, J.D., Gurnett, D.A., Hospodarsky, G.B., Braunger, R.M., Kintner, P.M., Kurth, W.S., 2001. Plasma waves observed in the cusp turbulent boundary layer: an analysis of high time resolution wave and particle measurements from the Polar spacecraft. J. Geophys. Res. 106 (A9), 19081–19099.

Pottelette, R., Treumann, R.A., 1998. Impulsive broadband electrostatic noise in the cleft: a signature of dayside reconnection. J. Geophys. Res. 103, 9299–9307.

Scudder, J., Hunsacker, F., Miller, G., Lobell, J., Zawistowski, T., Ogilvie, K., Keller, J., Chornay, D., Herrero, F., Fitzenreiter, R., Fairfield, D., Needell, J., Bodet, D., Googins, J., Kletzing, C., Torbert, R., Vandiver, J., Bentley, R., Fillius, W., McIlwain, C., Whipple, E., Korth, A., 1995. Hydra—a 3-dimensional electron and ion hot plasma instrument for the Polar spacecraft of the GGS mission. Science 71, 459–495.

Scudder, J.D., Mozer, F.S., Maynard, M.C., Russell, C.T., 2002. Fingerprints of collisionless reconnection at the Separator: I. Ambipolar-Hall signatures. J. Geophys. Res. 107 (A10), 1294.

Sonnerup, B.U.O., 1980. Theory of the low latitude boundary layer. J. Geophys. Res. 85, 2017–2026.

Treumann, R., LaBelle, J., Bauer, T., 1995. Diffusion processes: an observational perspective. In: Song, P., Sonnerup, B., Thomsen, M., (Eds.), Physics of the Magnetopause. Geophys. Monogr. 90, American Geophysical Union, Washington, DC, pp. 331–341.

Tsurutani, B.T., Thorne, R.M., 1982. Diffusion processes in the magnetopause boundary layer. Geophys. Res. Lett. 9, 1247–1250.

Umeda, T., Omura, Y., Matsumoto, H., Usui, H., 2002. Formation of electrostatic solitary waves in space plasmas: particle simulations with open boundary conditions. J. Geophys. Res. 107 (A12), 1449.

Winske, D., Thomas, V.A., Omidi, N., 1995. Diffusion at the magnetopause: a theoretical perspective. In: Song, P., Sonnerup, B., Thomsen, M. (Eds.), Physics of the Magnetopause. Geophys. Monogr. 90, American Geophysical Union, Washington, DC, pp. 321–330.